Volume 8 Number 10 1980 Nucleic Acids Research

Yeast $tRNA^{Phe}$ conformation wheels: a novel probe of the monoclinic and orthorhombic models

A.R.Srinivasan and W.K.Olson*

Department of Chemistry, Rutgers University, New Brunswick, NJ 08903, USA

Received 28 February 1980

ABSTRACT

A series of conformation wheels is constructed from the recently refined X-ray crystallographic data of monoclinic and orthorhombic yeast $tRNA^{Phe}$. These circular plots relate the primary chemical structure (i.e., base sequence) directly to the secondary and tertiary structure of the molecule. The circular sequence of backbone torsion angles displays a unique pattern that is useful both in distinguishing the ordered and disordered regions of the molecule and in comparing the three sets of experimental data. Composite conformation wheels describe the fluctuations in the "fixed" parameters (ϕ', ϕ, X) and independent conformation wheels reveal the changes in the "variable" parameters (ω', ω, ψ, ψ') of the three different yeast $tRNA^{Phe}$ models. Additional plots of base-stacking parameters help to visualize the intimate interrelationship between chemical sequence and three-dimensional folding of yeast $tRNA^{Phe}$. The composite data illustrate several conformational schemes that position the bases of adjacent nucleosides in a parallel stacked array and reveal an even larger number of conformations that introduce bends or turns in the polynucleotide chain.

INTRODUCTION

The recent X-ray crystallographic analyses of yeast $tRNA^{Phe}$[1-3] provide a wealth of information regarding both the organization of this particular family of molecules and the principles governing the folding of polynucleotides in general. In all reported structures, including most recently those of yeast $tRNA^{Gly}$,[4] eukaryotic initiator $tRNA_f^{Met}$,[5] E. coli $tRNA^{Arg}$,[6] and E. coli initiator $tRNA_f^{Met}$,[7] the molecule assumes a distinctive three-dimensional "L" shape. The various tRNA species also adopt characteristic organizational features including base-stacking, base-pairing, and base-interdigitation (i.e., pseudo-intercalation).[8]

Despite these similarities in gross morphology, close analysis of the three sets of refined X-ray coordinates[9-11] uncovers subtle but important differences in the local conformations of the tRNA structures. These variations arise principally from the several possible ways of fitting the molecular models to the electron density maps. This uncertainty in assigning

conformations stems from the fact that the atomic resolution of the crystallographic data (to 2.3-2.4 Å) is not at the level of refinement of chemical architecture (~1.5 Å).

Recently Srinivasan and Yathindra,[12] using the preliminary atomic coordinates of the monoclinic yeast $tRNA^{Phe}$ crystal,[13] constructed a conformation wheel to describe the secondary structure of this model. This simple representation markedly facilitates comprehension of the numerical rotation angle data compiled in the X-ray literature. The circular diagram presents the secondary conformational variations in the nucleic acid backbone as a function of the primary chemical sequence of bases. The resultant conformational sequence of double-stranded stems and single-stranded bends describes a unique two-dimensional "starburst" that complements the three-dimensional L-shaped representation of the molecule. The analysis additionally reveals conformational trends in the $tRNA^{Phe}$ molecule that may subsequently prevail in the spatial organization of other nucleic acid systems.

In this report we extend this graphic procedure to describe and compare the conformations of yeast $tRNA^{Phe}$ in the three recently refined sets of atomic coordinates.[9-11] We present both rotation angle wheels that follow the path of the tRNA backbone and stacking wheels that measure the association of adjacent bases. The similar sequences of rotation angles and stacking parameters affirm the general conformational resemblance of the three structures. Close examination of the conformation wheels, however, reveals subtle differences in nucleotide organization in the three models. These variations reflect the bias in the different data collection and computer model building procedures. The various ordered (stacked) and disordered (unstacked) conformers in the three models additionally provide useful estimates of flexibility in both helical and randomly coiling polynucleotide chains.

ROTATION ANGLE WHEELS

A conformation wheel illustrating the complete set of internal rotations reported by Hingerty *et al.*[9] for their refined monoclinic model of yeast $tRNA^{Phe}$ is presented in Fig. 1. The glycosyl (χ) and six backbone (ω', ω, ϕ, ψ, ψ', ϕ') rotations are displayed as a function of the sequence of bases in the molecule. An angular scale of 0° to 360° is constructed along the radii of the conformation wheel and the base sequence is displayed along the circumference of the wheel. The backbone angles are defined relative to the *cis* conformation as 0° and the glycosyl angle is determined

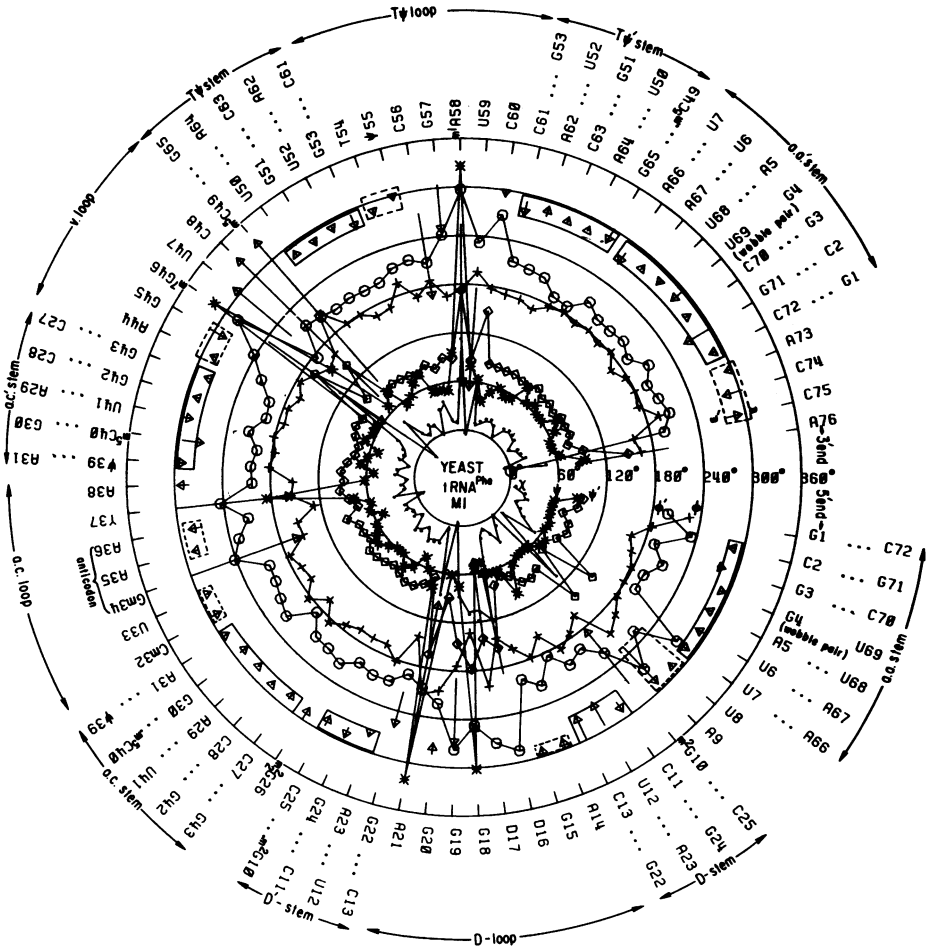

Figure 1
Conformation wheel of the M1 form of yeast $tRNA^{Phe}$ showing the glycosyl torsion (χ) and the backbone rotations (ω', ω, φ, ψ, ψ', φ') in relation to base sequence. The base and the tip of the arrows represent the ω' and ω values, respectively. The respective symbols - dot, diamond, octagon, plus and asterisk - indicate the χ, ψ', φ', φ and ψ rotations.

with respect to a cis arrangement of atoms O(1')-C(1')-N(9)-C(8) in purines and atoms O(1')-C(1')-N(1)-C(6) in pyrimidines. With the exception of ω' and ω, each angle is identified by a special symbol and the successive symbols of the same type are connected along the chain sequence. The phosphodiester pair preceding each nucleoside is denoted by an arrow, the base and

tip of which represent the ω' and ω rotations, respectively. The arrows associated with stretches of single- and double-stranded A-type helices are enclosed by dashed and solid arches, respectively. The various loop and stem segments of the conventional cloverleaf fold of yeast $tRNA^{Phe}$ are designated along the circumference of the wheel. The hydrogen bonding schemes in the helical stems are noted also at the periphery in terms of the associated complementary bases.

The variation of angles in Fig. 1 is somewhat altered from the circular plot reported for the unrefined monoclinic coordinates.[12] The ψ' and φ torsions are not explicitly included in the earlier figure. More importantly, the starburst pattern of the conformational sequence is markedly changed in the refined wheel. As noted by Hingerty et al.,[9] major variations are found in the loop regions of the two models.

The angular parameters described in Fig. 1 can be categorized as either "fixed" or "variable". Each of the "fixed" φ', φ and X variables is confined principally to a single range of conformation space. In contrast, the "variable" ω', ω, ψ and ψ' torsions are spread over several conformational domains. These conformational classifications are at once apparent from the conformation rings[14] displayed in Fig. 2. Here, the composite occurrences of various rotation angles of the three refined tRNA models are represented, after Sundaralingam,[15] in a series of concentric rings. Each ring is scaled from 0° to 360° and the occurrences of given conformation angles are represented by radial lines. The preferred conformational domains of each angle are apparent from the sectors with dense radial lines. The X, φ', and φ torsions are spread over relatively narrow ranges of angles compared to the variations of ω', ω and ψ. Greatest flexibility is seen in the ω angle which is distributed over the entire range of conformations. The relatively narrow range of the ψ' angle is associated with two distinct conformations of the pentose ring, the C3'-endo pucker where ψ' ~90° and the C2'-endo pucker where ψ' ~150°.

As illustrated below, the two angular categories of "fixed" and "variable" parameters are useful in the comparison of backbone conformations in the three refined models of yeast $tRNA^{Phe}$. The "fixed" parameters are compared individually on three composite conformational wheels while the "variable" angles are presented separately for each X-ray model. For simplicity, the three data sets are referenced below as M1 for the monoclinic data of Hingerty et al.,[9] M2 for the monoclinic data of Stout et al.,[10] and O1 for the orthorhombic model of Sussman et al.[11]

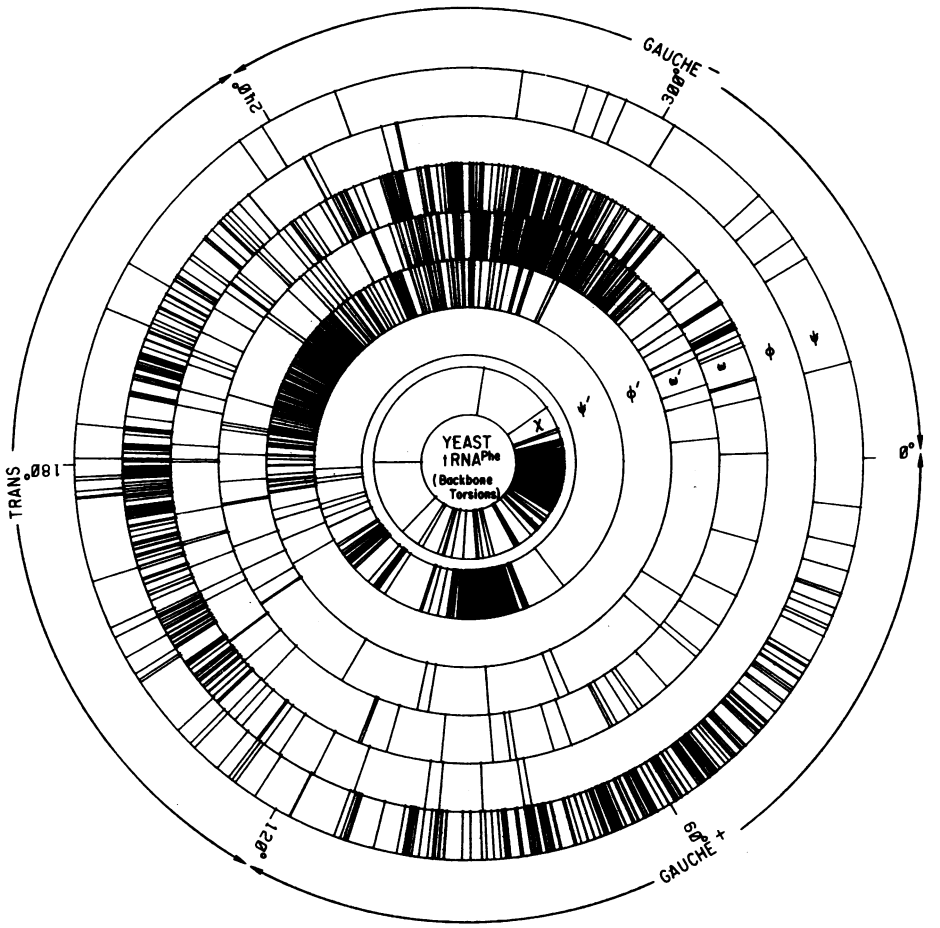

Figure 2
Conformation rings depicting the occurrences of internal rotations (χ, ψ', φ', ω', ω, φ, ψ) in the M1, M2, and O1 models of yeast $tRNA^{Phe}$. Rotational states are classified at the periphery of the outer ring as trans, gauche$^+$ or gauche$^-$. Note that the conformation wheel is rotated 90° in the clockwise direction from the conventional diagram.[15]

FIXED PARAMETER WHEELS

Composite conformation wheels describing the variations of the C(4')-C(3')-O(3')-P rotation (φ') and the P-O(5')-C(5')-C(4') rotation (φ) in the M1, M2, and O1 models are presented in Figs. 3(a) and 3(b), respectively. The parameters associated with the three models in each figure

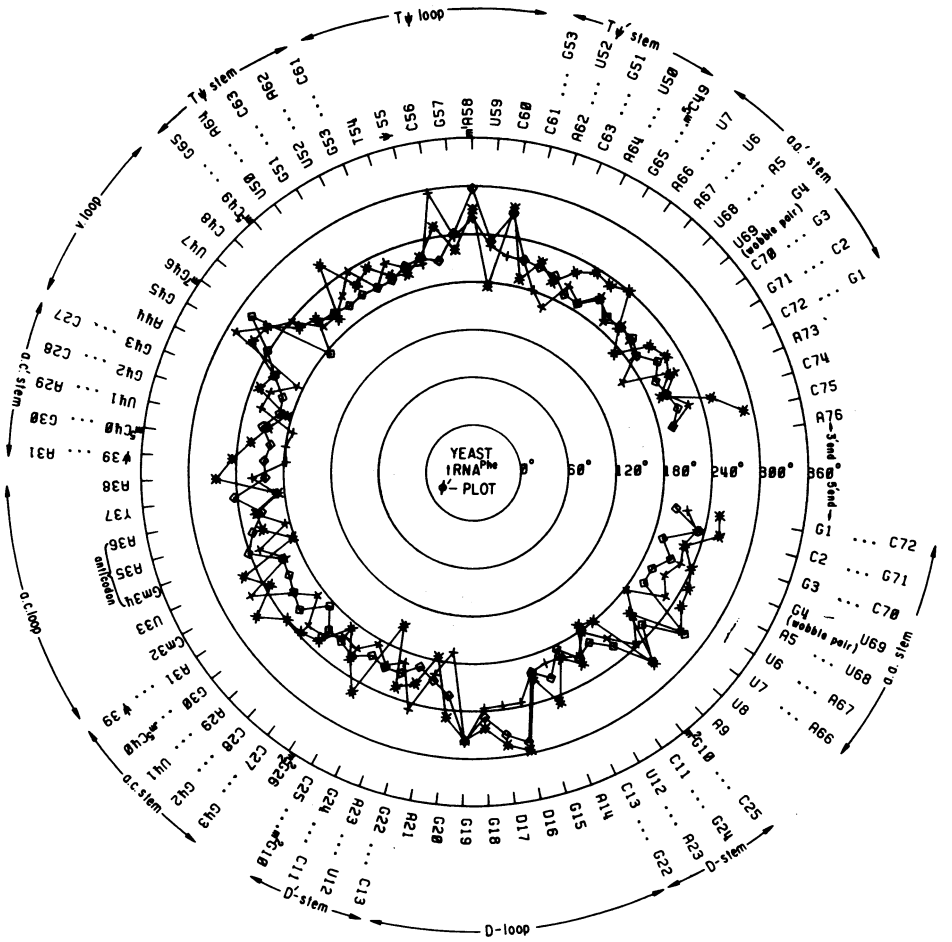

Fig. 3a

are represented by a diamond symbol (M1), a plus sign (M2), and an asterisk (O1). As evident from the figures, the ϕ' and ϕ angles are confined in all three molecules almost overwhelmingly to conformations not far removed ($\leq 60°$) from the planar trans (180°) state. The ϕ' angles, however, are clustered in the upper trans range between 180° and 240° and are consequently greater in magnitude than the ϕ angles which are spread between 120° and 240°. The mean values and average deviations of ϕ' and ϕ based upon the composite data are 219° ± 29° and 175° ± 30°, respectively. The ϕ' rotation is notably displaced to the gauche$^-$ or g$^-$ range centered at 300°

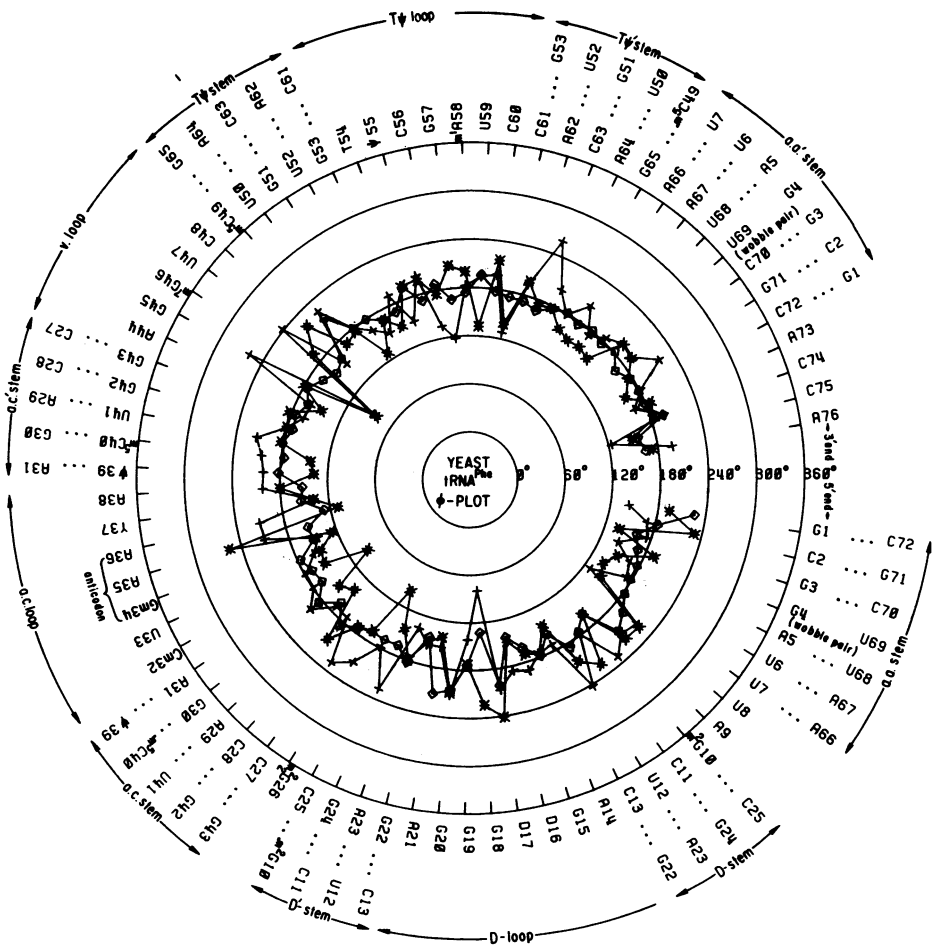

Fig. 3b

in the loop regions of the three models. In addition, the ϕ angle is found in the gauche$^+$ or g^+ range centered at 60° in certain loop regions of the M2 and O1 models. In the loops of the M1 model, the ϕ parameter is observed to parallel the g^+ deviations of the M2 and O1 data while being confined to the trans domain.

Close inspection of Figs. 3(a) and 3(b) reveals a striking "rigidity" in the model M1. In comparison to the M2 and O1 data, the M1 ϕ' and ϕ angles span a more restricted range of values. Indeed, within the helical

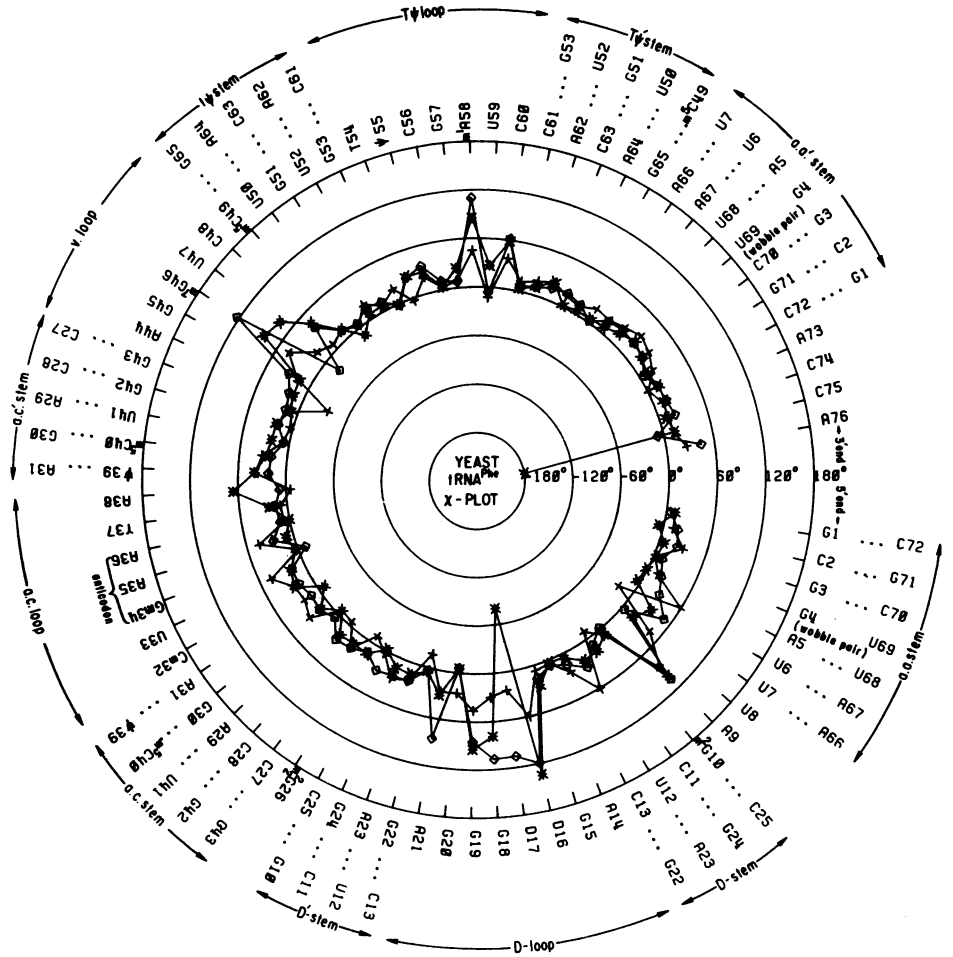

Fig. 3c

Figure 3
Composite conformation wheels showing the variation of (a) ϕ' (b) ϕ, and (c) χ with base sequence. The M1, M2 and O1 data are indicated respectively by diamond, plus and asterisk symbols.

stem regions of M1, the ϕ' and ϕ values closely match the ~210° and ~180° values that are associated with X-ray fiber diffraction models of RNA and synthetic polyribonucleotides[16] and that are also utilized as rotational isomeric states in theoretical models[17-18] of nucleic acids. In contrast,

the ϕ' and ϕ values are much less regular in the helical stems of the M2 and O1 models.

The variations of the glycosyl angle χ as a function of yeast $tRNA^{Phe}$ base sequence are represented in Fig. 3(c). The three X-ray models are distinguished by the same symbols used in Figs. 3(a) and 3(b). An altered radial scale of $-180°$ to $+180°$ is chosen for the χ conformation wheel to emphasize the relative rigidity of this parameter and also its interrelationship to the ϕ' and ϕ angles. According to Fig. 3(c), the χ angle is uniformly restricted to the normal anti (0-$60°$) range of values in the single- and double-stranded helical regions of the tRNA. Changes in the glycosyl angle that parallel the above cited variations in ϕ' and ϕ, however, are observed in the loop regions of the three models. These changes are most pronounced in the M1 and O1 data and are generally located in the high anti range centered about $\chi = 120°$. Apparently large distortions of χ are required to compensate for the minor conformational variations of ϕ' and ϕ in the loop regions of the M1 model. In contrast, the loop variability of χ in the O1 model, are comparable in magnitude to the large flexibility of ϕ' and ϕ. Indeed, two occurrences of syn glycosyl conformers are found in the orthorhombic data set at D17 in the dihydro uridine loop and at A76 in the CCA helical stem.

VARIABLE PARAMETER WHEELS

Conformation wheels describing variations in the ω', ω, ψ and ψ' rotation angles of yeast $tRNA^{Phe}$ are represented in Figs. 4(a)-(c). The data are presented separately for each of the three models rather than in the composite angular format of Fig. 3. The model format is chosen to emphasize both the strong interdependence of the four variable rotations within the nucleotide units of tRNA and the interrelationship of these angles to the primary sequence of nucleic acid bases. Comparison of $\omega'\omega$ pair values among the three structures is also facilitated by this scheme. The differences among the ψ' or ψ angles are much more easily distinguished than those associated with ϕ', ϕ, or χ in an analogous plot. By the fortuitous choice of the 0-$360°$ radial scale of values, these two parameters are concentrated primarily near the center of each ω', ω, ψ, ψ' wheel; consequently, deviations of ψ' and ψ from the predominant values are stressed by the graphs. The four variables on each wheel are designated by the same symbols utilized in Fig. 1.

The predominant conformation of the phosphodiester linkages in all three

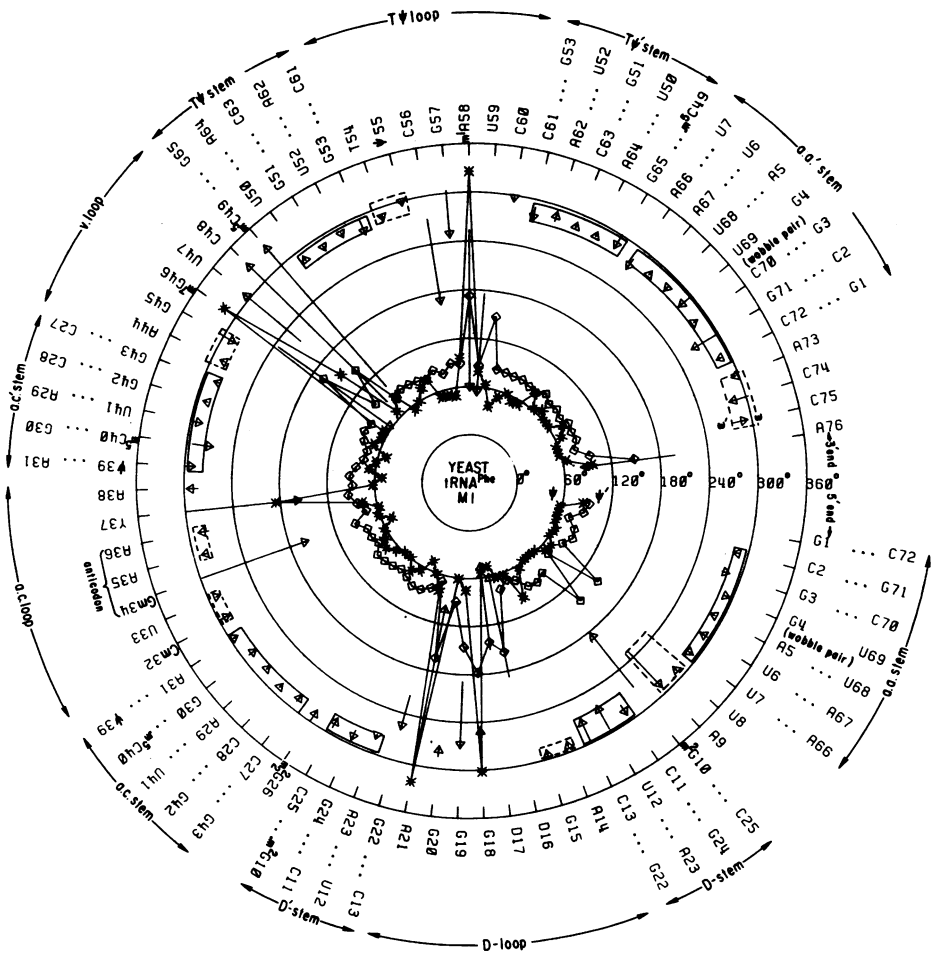

Fig. 4a

$tRNA^{Phe}$ models is the $\omega'\omega = \underline{g}^{-}\underline{g}^{-}$ state typical of ordered polynucleotides. The chain is organized as an A-type helix in the double-stranded stems and also in the single-stranded loops. Indeed, the A-type double helix is found to continue uninterrupted as a single strand over 2-5 nucleotides in the various tRNA loops. The minor fluctuations in arrow lengths on the conformation wheels are indicative of the non-regularity of the various helical fragments. In fact, the two complementary single-strands forming the double-helical stems are found to be conformationally dissimilar in all

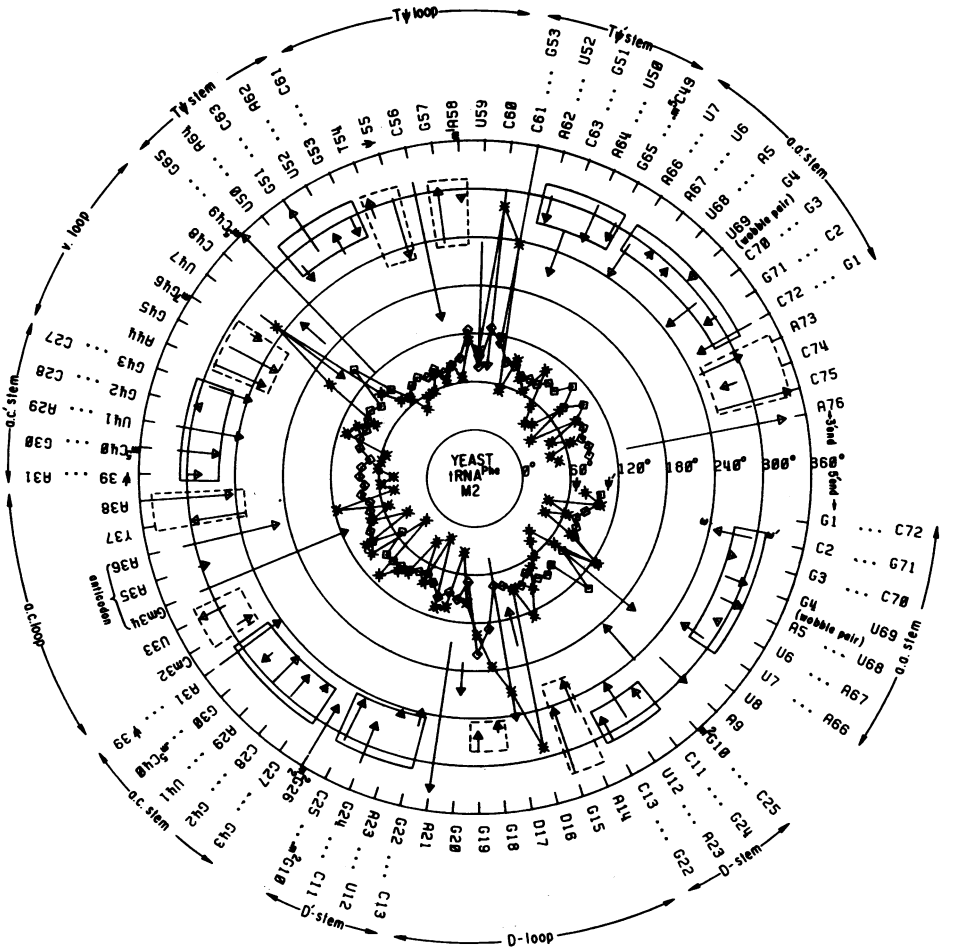

Fig. 4b

three X-ray models. Interestingly, the deviations of ω' and ω from helical regularity are least pronounced in the molecular model M1. Alternative non-A-type combinations of the ω' and ω angles are observed in the single-stranded loop regions. These states are required to fold the loops into hairpin bends. As evident from Figs. 4(a)-(c) and outlined in detail below, these bends can be constructed by several distinct conformational schemes. The angular variations of the various schemes may involve only one nucleotide as in the anticodon bends of the M1 and M2 models or may

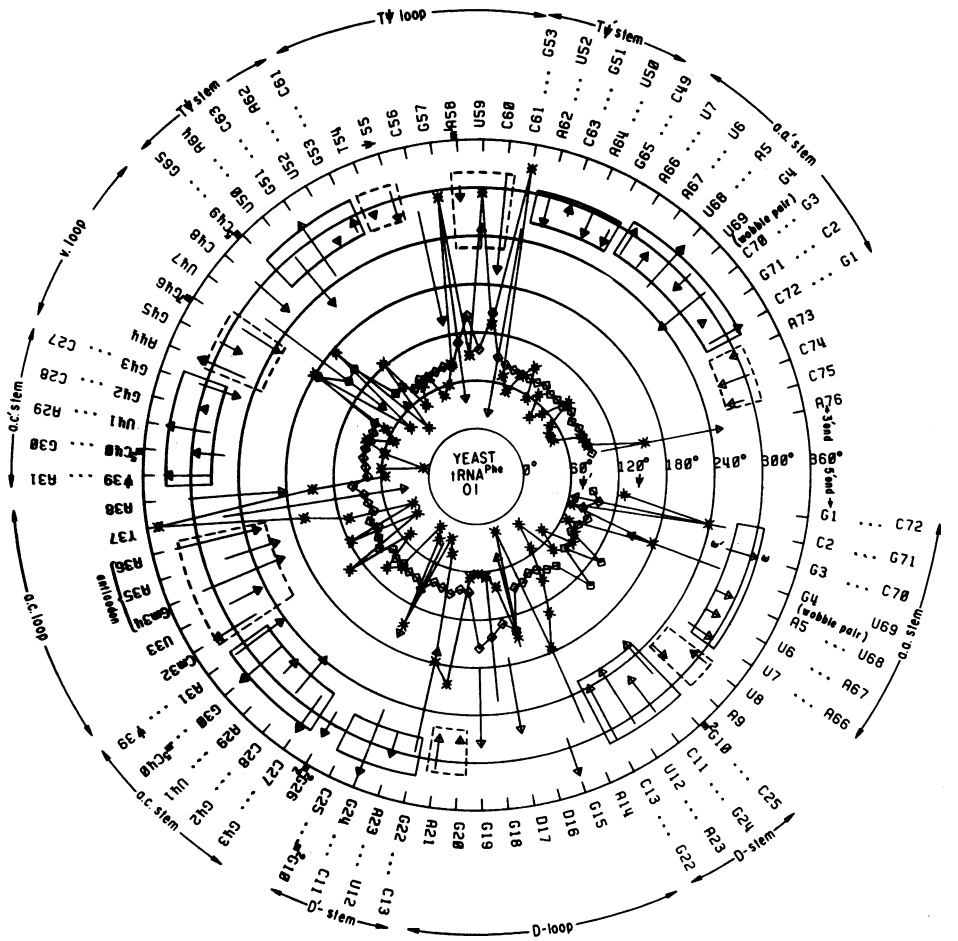

Fig. 4c

Figure 4
Conformation wheels showing the dependence of ω'ω (base and tip of the arrows), ψ (asterisk) and ψ' (diamond) with base sequence (a) M1 data (b) M2 data (c) O1 data.

spread over many residues as in the TψC loop of the O1 model. The various conformational distortions of ω' and ω in the tRNA hairpin bends are more pronounced than the relatively minor deviations in φ', φ, and X noted above in Fig. 3.

The ribose moieties of the tRNA models occur principally in the ψψ' =

g^+g^+ conformation. This rotational combination positions atom O(5') of each sugar in a gauche orientation with respect to the O(1') and the C(3') atoms of a C3'-endo puckered ring. Steric constraints of the ribose ring upon the ψ' angle account for the relative regularity of this parameter in the helical domains of all three conformation wheels. The ψ angle appears to be an equally regular variable over these base sequences in M1. Sizeable deviations (~60°) of the ψ angle, however, occur in corresponding helical residues of both the M2 and O1 models. Major deviations in ψ and ψ' accompany the drastic rotational changes of ω' and ω in the tRNA loops. The ψ angle may adopt a t or g^- state in the various bends while the ψ' angle may flip to the t range associated with C2'-endo puckering. (The $\psi' = g^-$ conformation is sterically unattainable to the 5-membered pentose ring). The M2 model also includes values of ψ' (~120°) associated with the unusual O1'-endo puckering. No examples of O1'-endo puckered ribose, however, exist among the reported X-ray structures of low molecular weight RNA analogs. This conformation positions atoms O(2') and O(3') in a sterically unwieldy eclipsed arrangement.

INTERDEPENDENCE OF ψ', ω', ω, ψ TORSIONS

The strong interdependence of consecutive ψ', ω', ω and ψ rotations suggested by the conformation wheels of Fig. 4 is organized quantitatively in Table 1. Each conformation angle has been classified as g^+ (0-120°), t (120-240°), or g^- (240-360°) and the composite frequency of occurrence of adjacent rotational combinations ($\psi'\omega'$, $\omega'\omega$, and $\omega\psi$) has been compiled from the three X-ray models. The results are presented as percentages for each angle pair in Table 1. As expected for a molecule that contains a large proportion of RNA-A helix, the $\psi'\omega'\omega\psi = g^+g^-g^-g^+$ state is preferred with

Table 1. Composite frequency of occurrence of rotation angle pairs.

ψ' \ ω'	g^+	t	g^-
g^+	2	5	81
t	1	5	6
g^-	6	14	67

ω' \ ω	g^+	t	g^-
g^+	0	0	3
t	3	2	5
g^-	6	14	67

ω \ ψ	g^+	t	g^-
g^+	4	2	4
t	10	6	0
g^-	69	4	1

an overall frequency of 61%. According to Table 1, the correlations between successive angle pairs are even higher than this figure; the $\psi'\omega'$ = $\underline{g}^+\underline{g}^-$ frequency is 81%, the $\omega'\omega$ = $\underline{g}^-\underline{g}^-$ frequency 67%, and the $\omega\psi$ = $\underline{g}^-\underline{g}^+$ frequency 69%. Although the occurrence of ψ' = $\underline{t}$ or C2'-endo states is rare, the ω' angle is seen to vary with a change in ring puckering. For C2'-endo residues the ω' = $\underline{t}$ and ω' = $\underline{g}^-$ states are approximately equally favored (5% and 6% respectively), while for C3'-endo residues the overwhelming preference of ω' is the $\underline{g}^-$ state (81% compared to 2% and 5%). A similar correlation of the $\psi'\omega'$ pair is suggested both by the d-pApTpApT crystal structure[19] and by semiempirical[20,21] and PCILO[22] energy calculations on ribodinucleoside triphosphate segments. A similar "long range" correlation of consecutive $\omega\psi$ rotations is further evident from the $\omega\psi$ matrix in Table 1. With ψ in the preferred $\underline{g}^+$ range, ω is found principally in a $\underline{g}^-$ state (69% compared to 10% and 4%). When ψ is varied to the $\underline{t}$ or $\underline{g}^-$ state the preferred value of ω is $\underline{t}$ or $\underline{g}^+$, respectively. The $\omega\psi$ rotation angle interdependence is also predicted by semiempirical[21] and PCILO[22] calculations on dinucleoside triphosphate and also by semiempirical minimization studies of d-pApAp.[23] According to the $\omega'\omega$ matrix frequencies in Table 1, conformational variations of the phosphodiester from the preferred $\underline{g}^-\underline{g}^-$ domain are most likely to entail, only a single angle. These changes to $\underline{t}\,\underline{g}^-$, $\underline{g}^+\underline{g}^-$, $\underline{g}^-\underline{t}$ and $\underline{g}^-\underline{g}^+$ states together with the favored $\underline{g}^-\underline{g}^-$ domain account for 95% of the phosphodiester states.

BASE-STACKING WHEELS

The seven rotatable bonds comprising each repeating unit of the polynucleotide chain provide a large variety of ways to organize the bases and backbone. Consequently, the compilation of torsion angles alone does not suffice to characterize the organization of nucleotides in yeast $tRNA^{Phe}$. As detailed below, there are several combinations of rotations in the three X-ray models that position the bases in parallel stacks and an even larger number of states that introduce bends in the chain.

The extent of base organization observed in the three tRNA models is illustrated by the three base-stacking conformation wheels in Figs. 5(a)-(c). Three stacking parameters - the angle Λ formed by the normals of adjacent base planes, the mean distance <Z> between planes of successive bases, and the mean pairwise separation <D> between atoms in adjacent planes - are reported separately as functions of base sequence.

The composite variations of Λ in the three models are reported in Fig.

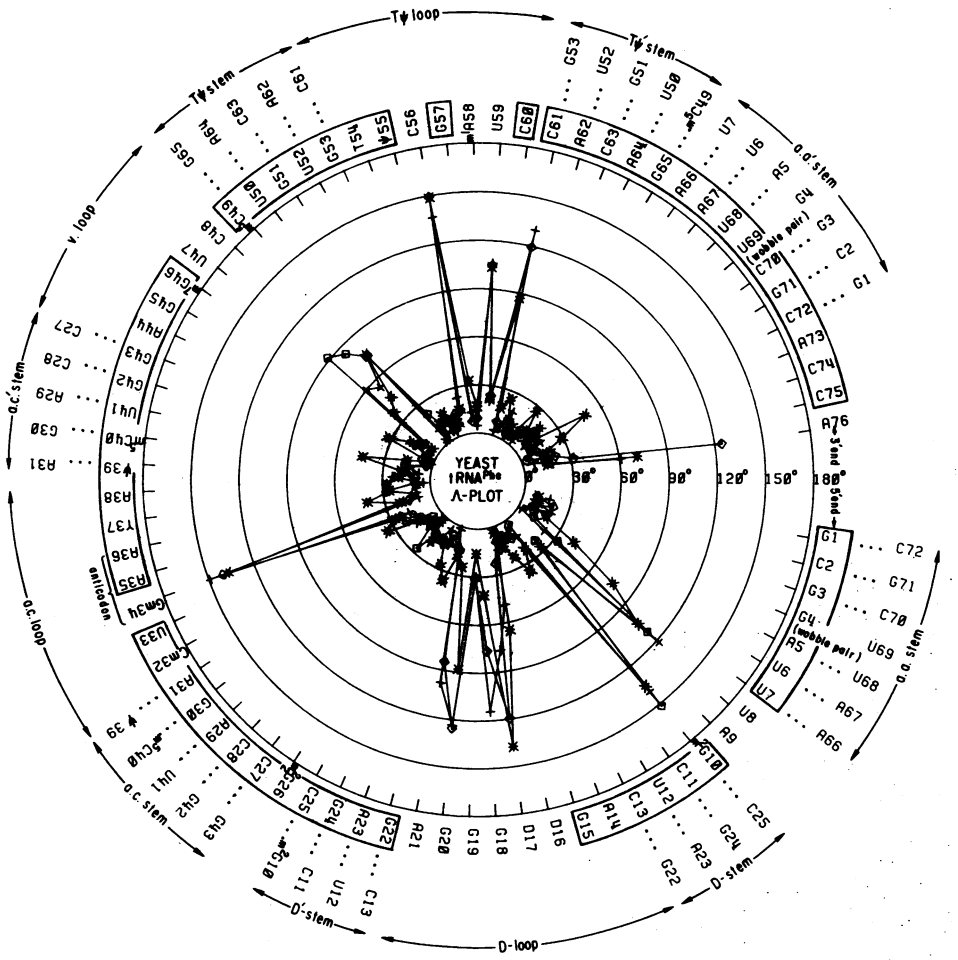

Figure 5(a)
Composite conformation wheel of the angle, Λ, between successive base planes in the M1 (diamond), M2 (plus), and O1 (asterisk) models. Units found to meet criteria of base-stacking (see text) are enclosed in boxes at the circumference of the wheel.

5(a). In this plot the set of symbols presented in Fig. 3 are again utilized to distinguish the three models. The radii are scaled from 0° at the center to 180° at the periphery of the circle. The value of Λ describing the orientation of each XpY dimeric unit is denoted at the Y or 3' position on the graph. As expected, the bases within the helical stems are confined to orientation angles in the range 0-30° corresponding to parallel arrange-

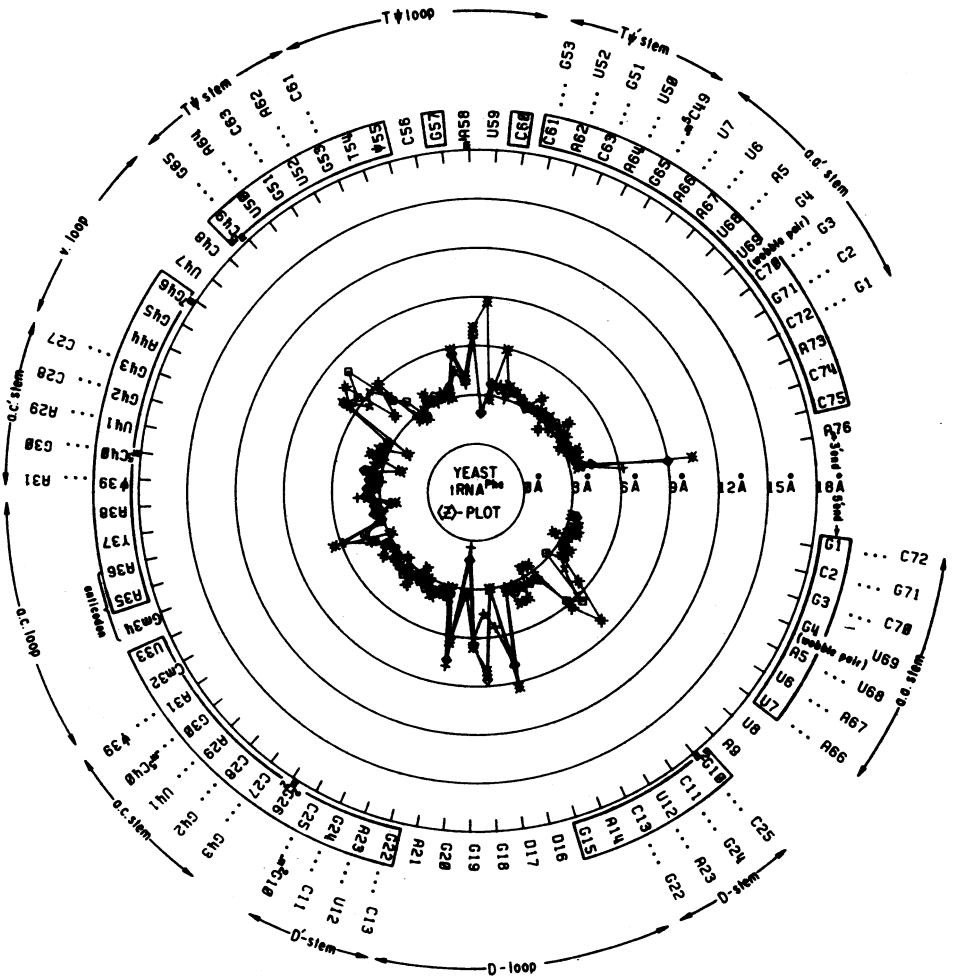

Figure 5(b)
Composite plot of the average perpendicular distance, <Z>, between successive base planes. See legend to Fig. 5(a).

ments. In the loop domains of the molecule, however, the values of Λ change abruptly. The pattern of spikes in the Λ conformation wheel is complementary to the "starburst" describing the sequence of torsion angles in Figs. 1, 3, and 4. The longest spikes corresponding to $\Lambda \sim 150°$ in Fig. 5(a) are indicative of chain reversals in the polynucleotide backbone. Such reversals are expected to unstack adjacent bases and also to enhance the

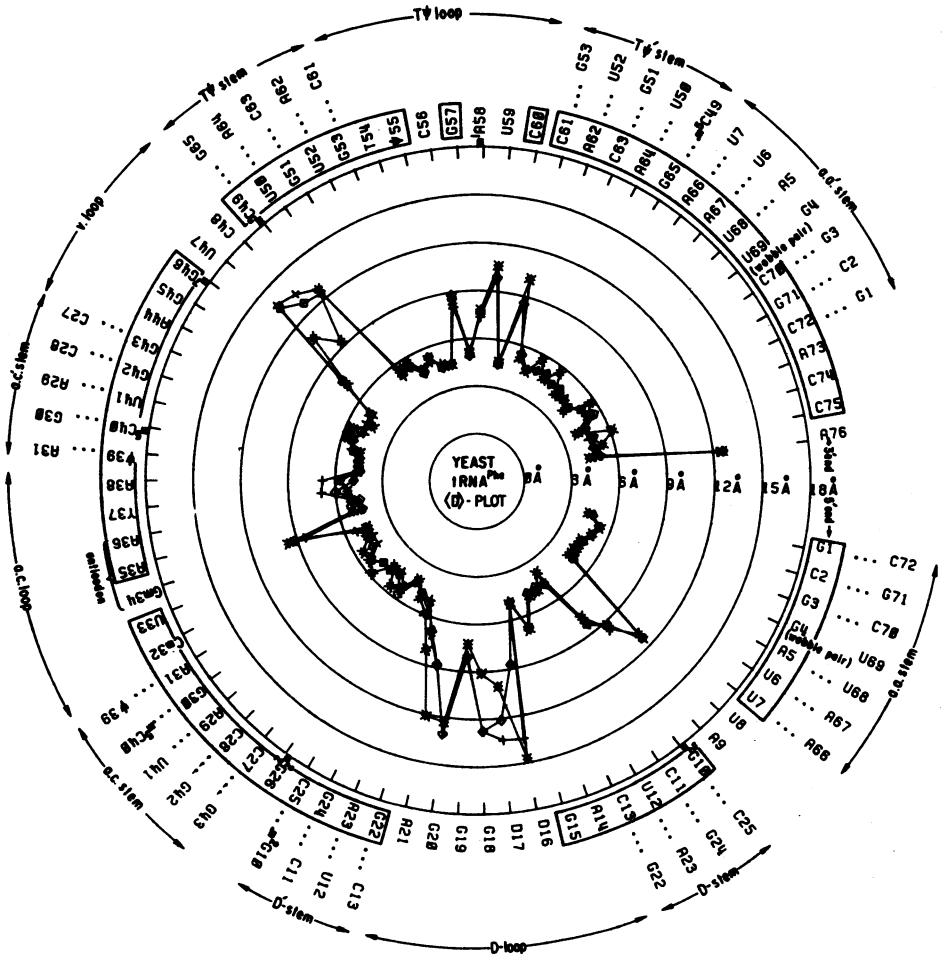

Figure 5(c)
Composite plot of the average pair-wise interatomic distance, <D>, between successive base planes. See legend to Fig. 5(a).

formation of hairpin turns in the polynucleotide backbone. The shorter spikes corresponding to Λ in the 60–90° range of the figure are indicative of sharp kinks that unstack bases and bend the polynucleotide backbone.

The distances, <Z> and <D>, represented in Figs. 5(b) and 5(c), respectively, also exhibit characteristic values in the helical stems of $tRNA^{Phe}$ and then sharply increase in magnitude in the loop domains. The radial

scale in these two plots extends from 0 to 18 Å. The ideally stacked values of <Z> and <D> are approximately 3.5 Å and 5.5 Å, respectively. The <D> parameter, which is a measure of base overlap, will generally exceed the value of <Z>. The two distances become similar, although never identical, when the bases of a homodimer (XpX) assume a perfectly parallel orientation (i.e., $\Lambda = 0°$) and thus coincide in one planar projection (i.e., 100% overlap). In the loops of the tRNA model, <Z> increases to values of 7 Å or more typical of intercalation distances. The accompanying large increases in <D>, however, suggest that the bases may not always exhibit overlap.

As evident from Figs. 5(a), 5(b), and 5(c), the values of the stacking parameters are comparable in the three X-ray models. The major discrepancies are found in the hairpin loops and are noted mainly in the M2 data. Close, if not identical, similarities in Λ, <Z>, and <D> from the three models are expected since the location of base moieties is within the resolution of the X-ray data.

MOLECULAR ORGANIZATION OF BASES

The values of the base-stacking parameters observed in the yeast $tRNA^{Phe}$ crystals fall into four distinct configurational classes. The majority of sequential bases (168 out of the 225 possible dimer units = 75%) adopt a normal parallel stacking arrangement (S) where $\Lambda \leq 45°$, $3.0 \leq <Z> \leq 4.0$Å, and $4.5 \leq <D> \leq 5.5$Å. These S sequences are enclosed within boxes in Figs. 5(a)-(c). In some cases, however, the parallel bases open to an intercalated geometry (I) with $<Z> \geq 6$Å and $<D> \geq 7.5$Å that allows the intercalation of another planar species. In addition, there are a large number of unstacked dimer sequences that can be classified as either bends (B) or reversals (R). The B state where $\Lambda = 90 \pm 45°$ involves a smaller tilt of bases from the R state where $\Lambda \geq 135°$. Indeed, the bases adopt a parallel, although non-overlapping, arrangement in a reversal unit.

The four categories of dimer configurations offered here are indirectly related to the three kinds of polynucleotide backbone bends detailed recently by Ponnuswamy and Thiyagarajan.[24] As illustrated in the schematic in Fig. 6, our base-stacking categories reflect the separation of base planes in a dinucleoside triphosphate (or dinucleoside monophosphate) segment of the tRNA backbone. The states defined by Ponnuswamy and Thiyagarajan, on the other hand, depend upon the imaginary torsion angle Θ described by three consecutive backbone virtual bonds in either a trinucleoside tetraphosphate (illustrated in Fig. 6) or a trinucleoside diphosphate (reported

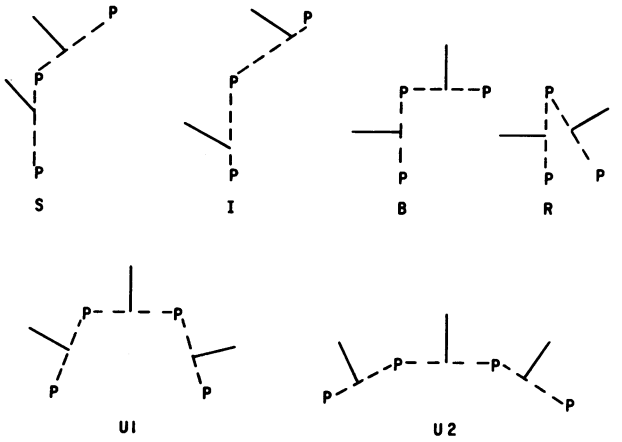

Figure 6
Schematic illustration of base-stacking and backbone bending in dinucleoside triphosphate and trinucleoside tetraphosphate chain segments. The dashed lines represent the hypothetic virtual bonds that connect successive phosphorous atoms. The solid lines approximate the attached bases.

in reference 24). In our opinion, the trimer bending categories are too loosely defined to relate the three-dimensional configuration of yeast $tRNA^{Phe}$ to local conformational changes. For example, as shown in Fig. 6, a sharp turn U1 of the trimer backbone with $\theta = 0^{\circ}$ (cis) involves two dimeric B states. In instances when the imaginary P-P-P valence angles approach 180°, however, such a turn (U2) may entail two normally stacked dimer units! Interestingly, both trimer U-turns illustrated in Fig. 6 follow less jagged paths than typical dimer reversal segments.

The crystallographic data reveal three distinct conformational combinations that position adjacent bases of the tRNA strand in a stacked array. The majority of S units adopt the energetically favored A-RNA helical conformation where $\psi'\omega'\omega\psi = \underline{g^+g^-g^-g^+}$, $\phi' = \phi = \underline{t}$, and $\chi = \underline{anti}$. In addition, there are 12 examples of A-type Watson-Crick base-stacking where $\psi'\omega'\omega\psi = \underline{g^+g^-t\ t}$ and one example of stacking where $\psi'\omega'\omega\psi = \underline{g^+g^-g^+g^-}$. The interdependence of ω and ψ in these three base-stacking categories results in a unique crankshaft motion of the polynucleotide that allows both backbone flexibility and base-stacking at the same time.[25]

There are 14 examples of intercalation geometry in the X-ray models of yeast $tRNA^{Phe}$. In all three data sets an I state occurs between G18-G19

in the D-loop and between G57-m^1A58 in the TψC loops. The intercalation sites in these two hairpin loops are also cleavage sites of T1 ribonuclease.[26] In addition, intercalated states occur in all three models in the juncture region of the tRNA "L" - between U8-A9 and between G45-m^7G46. Interestingly, the intercalated states involve conformational combinations of the polynucleotide backbone similar to those associated with normal base-stacking. Eleven of the I states entail either the A-type helical conformer or the related ωψ crankshaft conformers. The intercalation site between G18-G19 in all three models, however, involves typical B-type helical geometry (^{2}E-^{2}E sugar puckering).

We find 33 examples of dimer units that meet the broad definition of a bend. Most of these bends (23) arise by a single rotational change (in ω', ω, or ψ) from standard A- and B-type helical backbones. Eight of the bends involve changes in two angles (either ω'ω or ω'ψ) from the helical states while only two involve changes in three angles. Two of the bending sites (G19-G20 and G20-A21) are also T1 ribonuclease cleavage sites.

Chain reversals appear at three distinct sites in the yeast $tRNA^{Phe}$ molecule. All three data sets indicate R sites at A9-m^2G10 in the "L" juncture, G33-Gm34 of the anticodon loop, and ψ55-C56 of the TψC loop. All of these chain reversals entail either ψ'ω'ωψ = $\underline{g^+g^-tg^+}$ or ψ'ω'ωψ = $\underline{tg^-tg^+}$ backbone conformations. Interestingly, there are no examples of either the ψ'ω'ωψ = $\underline{tg^+g^+t}$ conformational reversal found in the zigzag d-$(pCpG)_3$ crystal[27] or the ψ'ω'ωψ = $\underline{g^+g^+g^+g^+}$ reversal observed in UpA^+.[28,29]

The different types of base arrangements that characterize the single-stranded segments of the yeast $tRNA^{Phe}$ crystal provide new insight into the flexibility of polynucleotide chains. As noted above, several different chain conformations, including the predominant A-RNA helix, permit the occurrence of base-stacking. No single non-stacked conformation appears to predominate over any other non-stacked state. For example, the three hairpin loops of tRNA span similar chain lengths but adopt distinctly different backbone conformations. In all three X-ray models eight of the nine dimeric segments that constitute the D-loop involve unstacking of bases. In contrast, only four of the eight dimer segments of the TψC loop models assume unstacked states. Despite the different three-dimensional features, the three hairpins meet the same stringent geometric criteria of loop closure (e.g. terminal Watson-Crick base pairing).

The compilation of base-stacking parameters additionally helps to comprehend the modes of action of T1 and S1 nucleases with yeast $tRNA^{Phe}$.[26] We

Table 2. Principal nuclease cleavage sites in yeast $tRNA^{Phe}$[26]

Ribonuclease T1		Endonuclease S1	
Sequence	Configuration[±]	Sequence	Configuration
G15-D16	I, B, B	U33-Gm34	R
G18-G19	I, I, I	A35-A36	S
G19-G20	B, B, B	A36-Y37	S
G20-A21	B, I, B	A73-C74	S
G57-m^1A58	I, I, I	C74-C75	S
		C75-A76	B

[±]M1, M2, O1

categorize the known cleavage sites of the two enzymes by base sequence and configuration in Table 2. Interestingly, the major T1 cleavage sites entail either bent or intercalated geometries that expose the bases and backbone. Despite the well-known specificity of T1 to cleave after guanine residues,[30] the enzyme does not affect the Gm34-A35 unit of the anticodon stem on the surface of the molecules. Apart from the resistance to T1 by the modified guanylic acid (Gm34),[31,32] this non-reactivity may also possibly reflect the occurrence of a normally stacked state at this position. In contrast, the S1 enzyme cleaves both S and altered conformers. As is well-known, this enzyme is specific to single-stranded domains.[33]

SUMMARY

The conformation wheels detailed above provide a clear and useful way to store, display, and compare the several sets of refined crystallographic data reported recently for tRNA. The circular sequence of torsion angles displays a unique conformational pattern that is far easier to comprehend than a table of comparative rotation angle data. The various yeast $tRNA^{Phe}$ wheels immediately reveal the degree or absence of bias in the different X-ray model building schemes. Additional plots of base-stacking parameters help to visualize the intimate interrelationship between chemical sequence and three-dimensional folding in the different polynucleotide chains. The composite data illustrate a variety of conformational schemes that fit the

observed electron densities. For example, at least three distinct chain conformations can position the bases of adjacent nucleosides in a stacked array. Various rotation angle combinations can also produce molecular bends and turns. Differences among the data sets arise primarily in the single-stranded loop regions. The X-ray models also offer widely different torsion angle sequences to describe the same three-dimensional molecular fold (such as the TψC, anticodon or D-loop). Principles of polynucleotide conformation deduced from a single yeast $tRNA^{Phe}$ data set, thus, may not necessarily hold for all three molecular models.

ACKNOWLEDGEMENTS

The authors are greateful to the National Institutes of Health (USPHS Grant GM20861) and the Charles and Johanna Busch Memorial Fund of Rutgers University for laboratory support; the Center for Computer and Information Services of Rutgers University for computer time; to Dr. B. Hingerty, Professor M. Sundaralingam, and the Brookhaven Protein Data Bank[34] for the tRNA data used in this report. W. K. Olson acknowledges a USPHS Career Development Award (GM00155) and fellowships from the Alfred P. Sloan Foundation and the John Simon Guggenheim Memorial Foundation.

*To whom correspondence should be sent.

REFERENCES

1. Kim, S.-H., Quigley, G.J., Suddath, F.L., McPherson, A., Sneden, D., Kim, J.J., Weinzierl, J. and Rich, A. (1973) Science 179, 285-288.
2. Robertus, J.D., Ladner, J.E., Finch, J.T., Rhodes, D., Brown, R.S., Clark, B.F.C. and Klug, A. (1974) Nature 250, 546-551.
3. Stout, C.D., Mizuno, H., Rubin, J., Brennan, T., Rao, S.T. and Sundaralingam, M. (1976) Nuc. Acids Res. 3, 1111-1123.
4. Wright, H.T., Manor, P.C., Beurling, K., Karpel, R. and Fresco, J.R. (1979) in Transfer RNA: Structure, Properties and Recognition, Cold Spring Harbor Laboratory, pp. 145-160.
5. Schevitz, R.W., Podjarny, A.D., Krishnamachari, N., Hughes, J.J., Sigler, P.B. and Sussman, J.L. (1979) Nature 278, 188-190.
6. Stout, C.D., Rubin, J., Brennan, T., Rao, S.T., McMullan, R.K. and Sundaralingam, M. (1975) in "Structure and Conformation of Nucleic Acids and Protein-Nucleic Acid Interactions", Proceedings of the Fourth Annual Harry Steenbock Symposium, Sundaralingham, M. and Rao, S.T., Eds., pp. 59-69, University Park Press, Baltimore.
7. Woo, N.H., Roe, B.A. and Rich, A. (1979) Amer. Cryst. Assoc. Abstracts, Boston, Massachusetts, August 12-17.
8. Sundaralingam, M. (1979) in Transfer RNA: Structure, Properties and Recognition, Cold Spring Harbor Laboratory, pp. 115-132.
9. Hingerty, B., Brown, R.S. and Jack, A. (1978) J. Mol. Biol. 124, 523-534.

10. Stout, C.D., Mizuno, H., Rao, S.T., Swaminathan, P., Rubin, J., Brennan, T. and Sundaralingam, M. (1978) Acta Cryst. B34, 1529-1544.
11. Sussman, J.L., Holbrook, S.R., Warrant, R.W., Church, G.M. and Kim, S.-H. (1978) J. Mol. Biol. 128, 607-630.
12. Srinivasan, A.R. and Yathindra, N. (1977) Nucleic Acids Res. 4, 3969-3979.
13. Jack, A., Ladner, J.E. and Klug, A. (1976) J. Mol. Biol. 108, 619-649.
14. A similar approach was proposed by Sundaralingam, M. (private communication).
15. Sundaralingam, M. (1969) Biopolymers 7, 821-860.
16. Arnott, S., Chandrasekaran, R. and Selsing, E. (1975) in "Structure and Conformation of Nucleic Acids and Protein-Nucleic Acid Interactions", Proceedings of the Fourth Annual Harry Steenbock Symposium, Sundaralingam, M. and Rao, S.T., Eds., pp. 577-596, University Park Press, Baltimore.
17. Yathindra, N. and Sundaralingam, M. (1974) Proc. Nat. Acad. Sci. USA, 71, 3325-3328.
18. Olson, W.K. (1975) Macromolecules 8, 272-275.
19. Viswamitra, M.A., Kennard, O., Jones, P.G., Sheldrick, G.M., Salisbury, S. and Falvello, L. (1978) Nature 273, 687-688.
20. Yathindra, N. and Sundaralingam, M. (1975) in "Structure and Conformation of Nucleic Acids and Protein-Nucleic Acid Interactions", Proceedings of the Fourth Annual Harry Steenbock Symposium, Sundaralingam, M. and Rao, S.T., Eds., pp. 649-676, University Park Press, Baltimore.
21. Srinivasan, A.R. and Olson, W.K. (unpublished results).
22. Broch, H. and Vasilescu, D. (1979) Biopolymers 18, 909-930.
23. Broyde, S. and Hingerty, B. (1979) Nuc. Acids Res. 6, 2165-2178.
24. Ponnuswamy, P.K. and Thiyagarajan, P. (1979) Biochem. Biophys. Res. Comm. 89, 374-385.
25. W. K. Olson (unpublished data).
26. Wrede, P., Wurst, R., Vournakis, J. and Rich, A. (1979) J. Biol. Chem. 254, 9608-9616.
27. Wang, A.H.J., Quigley, G. J., Kolpak, F. J., Crawford, J. L., van Boom, J. H., van der Marel, G. and Rich, A. (1979) Nature 282, 680-686.
28. Sussman, J. L., Seeman, N. C., Kim, S.-H. and Berman, H. M. (1972) J. Mol. Biol., 66, 403-422.
29. Rubin, J., Brennan, T. and Sundaralingam, M. (1971) Science 174, 1020-1022.
30. Sato, K. and Egami, F. (1957) J. Biochem. 44, 753-767.
31. McCully, K. S. and Cantoni, G. L. (1961) Biochem. Biophys. Acta 51, 190-192.
32. Raj Bhandary, U. L., Stuart, A. and Chang, S. H. (1968) J. Biol. Chem. 243, 584-591.
33. Wurst, R., Vournakis, J. and Maxam, A. (1978) Biochemistry 17, 4493-4499.
34. Bernstein, F. C., Koetzle, T. F., Williams, G.J.B., Meyer (Jr.), E. F., Brice, M. D., Rodgers, J. R., Kennard, O., Shimanouchi, T. and Tasumi, M. (1977) J. Mol. Biol. 112, 535-542.